6(2009) 413 – 440

Latin American Journal of Solids and Structures

www.lajss.org

Response of axially stacked square tubes to axial impact loads

Abstract

The crushing and energy absorption characteristics of thin-walled specimens consisting of single and axially stacked mild steel square tubes are investigated by the performance of quasi-static and dynamic axial crushing tests. Two tubes are axially stacked either by means of weld or a plate. Welded specimens comprise of two tubes of equal length axially stacked on each other and seam welded around all four sides. Plate divided specimens consist of two tubes of equal length axially stacked with a rigid mild steel plate in between them. The rigid plate has a thickness of 10mm and acts as an elastic medium for energy to be transferred from the top tube to the bottom tube during axial loading. All tubes have square cross-sections of 50mm×50mm and nominal wall thicknesses of 1.6mm. The lengths of the tubes range from 250mm to 1700mm encompassing the three main modes of buckling; namely progressive, Euler and the transition mode. The global slenderness or length-to-width ratio (L/C) is investigated with regards to buckling modes. Welded tubes behave very similarly to single tubes. Plate-divided specimens exhibit two high peak loads with a slightly increased mean crush load compared to single and welded tubes.

Keywords

Progressive buckling, buckling transition, global bending, axially stacked, axial impact loading, tube crushing, energy absorber.

F. Ronchietto, S. Chung Kim Yuen* and G. N. Nurick

Blast Impact and Survivability Research Unit (BISRU), Department of Mechanical Engineering, University of Cape Town, Rondebosch, Private Bag, 7701 – South Africa

Received 7 Aug 2009;
In revised form 25 Oct 2009

* Author email:
steeve.chungkimyuen@uct.ac.za

1 INTRODUCTION

The pursuit for lighter and better energy absorbing devices has led to an increased awareness in the practicality of thin-walled sections. Such devices are very important in improving vehicle crashworthiness without increasing the weight of the vehicle. For vehicle occupants' safety it is desirable that the vehicle structure limits the deceleration, absorb the impact forces and maintains structural integrity [18, 19, 34, 35]. Other applications with regard to energy absorption include transportation bumpers and base of elevator shafts. Elevators have numerous safety devices such as electromagnetic brake systems. However, if all of these devices fail and the elevator does fall down the shaft, there is one final safety measure that may save

NOMENCLATURE

C	Mean width of square tube
CHS	Cross Head Speed
D	Cowper-Symonds coefficient
E_{pd}	Plastic deformation energy
H	Mean wall thickness of square tube
L_{bottom}	Unclamped length of bottom tube in plate-divided specimens
L_{top}	Length of top tube in plate-divided specimen
L	Total length of a specimen
M	Drop mass in dynamic tests
M_0	Plastic moment
P_m	Theoretical prediction of mean crushing load
P_m^d	Average value of dynamic crushing load
P_m^s	Average value of static crushing load
P_{ult}	Ultimate peak load
V_o	Impact Velocity of striking Mass
h	Drop height in dynamic tests
m	Mass of specimen
q	Cowper-Symonds exponent
δ	Total axial displacement of a specimen
δ_{bottom}	Displacement of bottom tube
δ_{top}	Displacement of top tube
σ_0	Mean value of plastic flow stress

the passengers. Typically the bottom of the shaft has a heavy-duty shock absorber system or thin-walled tubes system working like a giant cushion to soften the elevator car's landing.

An efficient energy absorption device would minimise the impact force and absorb as much energy as possible. In so doing the device will reduce the acceleration experienced by vehicle occupants and thus reduce the energy transferred to the occupants and cargo. Energy absorbers are vital in converting kinetic energy, resulting from impact, into other forms of energy such as large plastic deformations [4].

Extensive literature exists on theoretical, numerical and experimental studies on the axial crushing of tubular sections such as square and circular sections as discussed in detail by various authors [2, 3, 20, 23–25]. While most investigations deal with steel tubular structures, lightweight materials such as aluminium are also popular energy absorbers [25–27, 34]. Geometric changes to improve the energy absorption characteristics of tubular structures include additions such as fillers and imperfections. In the case of fillers the investigations are focused on a single tube with a filler such as aluminium foam [16, 33] or wood [32]. Seitzberger *et al.* [33] investigated the effects of different tube and filler arrangements on the crushing behaviour of axially compressed tubular crush elements, including two tubes in parallel with aluminium foam. Other authors that have investigated the response of more than one tubular structure

subjected to an axial load include Chung Kim Yuen *et al.* [13], who investigated the energy absorption characteristics of double-cell tubular profiles of different cross-sections. Theobald and Nurick [36] reported on the efficiency of multiple thin-walled tubes in parallel placed between steel plates and subjected to blast loading. Many papers have been published by a variety of authors on the effects of imperfections on the buckling effect of square tubes. These imperfections include pre-buckle [26], corner and dished indentations[1, 31], cutouts [6–8, 15], triggered dents [14, 28, 29] and blast dents [9, 11, 12]. An overview of the energy absorbing characteristics of tubular structures with geometric and material modifications has been presented by Chung Kim Yuen and Nurick [10]. Hitherto no studies have been reported on thin-walled tubes axially stacked in series.

When tubular structures are subjected to axial loads, the two main modes of failure are Euler and progressive buckling. Euler buckling occurs in relatively long, slender tubes and is characterised by large inelastic global bending while progressive buckling is typically associated with the formation of lobes during crushing of relatively short tubes. The progressive buckling mode is the most efficient energy absorbing form of collapse in tubes because most of the material is utilised in energy absorption through plastic work. Classifications of modes of failure are well established [2, 18]. In the context of tube crushing, one area of particular interest is the transition from Euler to Progressive buckling. Transition buckling is a distinct mode under dynamic loading whereby a tube begins to buckle progressively and then continues to bend globally or vice versa. Various authors [3, 5, 17, 21, 22] have carried out experimental and numerical studies to investigate this occurrence. Andrews *et al.* [5] pioneered the study of transition buckling. In their study they performed experimental tests and were able to create a classification chart that describes the relationship between tube length and thickness to the buckling modes for cylindrical aluminium tubes. Abramowicz and Jones [3] also investigated this topic with their experimental study on static and dynamic axial crushing of square and circular steel tubes which buckled mostly in the plastic range. Their results varied considerably from those of Andrews *et al.* [5] because of the different materials used, steel and aluminium. Abramowicz and Jones [3] found that in general the transition from progressive to global buckling for a given thickness, given by the critical length-to-width ratio $(L/C)_{cr}$, was larger under dynamic loading than for quasi-static loading. Jensen *et al.* [17] also studied buckling transition but in aluminium tubes with various cross-sections and impact velocities. Their study emphasised the importance of material properties and inertia effects when characterizing buckling transition, and found that materials with high yield stress and low strain hardening perform better than materials with a low yield stress and high strain hardening.

In this paper, a study on quasi-static and dynamic axial loading of two tubes axially stacked in series is presented by an investigation of deformation modes and energy absorption. The lengths of the specimens encompass the progressive and transition buckling regions. The two configurations are also compared to single tubes of equivalent lengths to determine which of the configurations is the most efficient energy absorber.

2 TEST SPECIMENS

The test specimens consist of industrial seam welded square tubes made from mild steel and have nominal cross sections of 50mm×50mm and a wall thickness of 1.6mm. The experiments are carried out in three configurations. These configurations include single tubes, welded tubes and plate-divided tubes. The welded specimens consist of two tubes seam welded together at the ends of the two tubes by the process of Gas Tungsten Arc Welding (GTAW), more frequently referred to as TIG welding. Quasi-static and dynamic crush tests were performed with two tubes welded in different ways. These welded specimens included four-sided seam weld, four corner spot welds, four side spot welds and two sided seam welds as illustrated in Figure 1. In plate-divided specimens a rigid plate is centrally inserted between the two tubes to act as an elastic medium for energy to transfer from the top tube to the bottom tube during axial loading and as support for the top tube. The plate and top tube are simply placed and aligned in the same orientation as the clamped bottom tube without any bonding as shown in Figure 2a. Preliminary quasi-static and dynamic crush tests were performed with axially stacked tubes without the rigid plate. In these tests the top tube always slipped and produced undesirable results as the tubes tore into one another as shown in Figure 2b, leading to the insertion of the rigid mild steel plate. The plate has dimensions of 75mm×75mm with a thickness of 10mm.

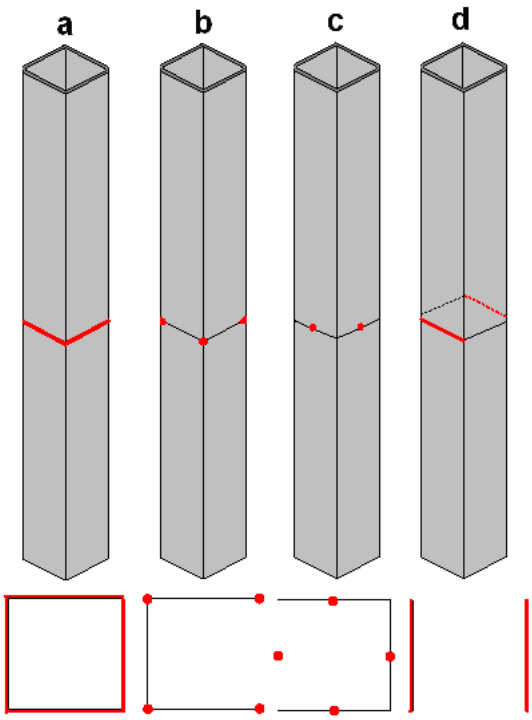

Figure 1 Weld configurations: (a) four-sided seam weld, (b) four corners spot welds, (c) four-sided spot welds and (d) two-sided seam weld.

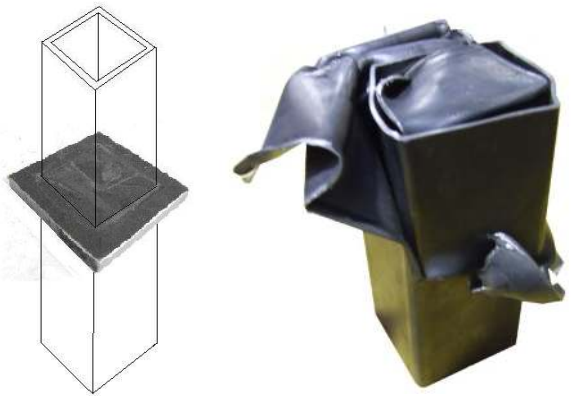

(a) (b)

Figure 2 (a) Rigid plate which was inserted between the top and bottom tube of each plate divided specimen and (b) tearing of two tubes without a rigid plate in between the two tubes.

Tensile test specimens, cut from the tubes walls, are tested at strain rates in the range from10-2/s to 10-3/s at room temperature. Using the Cowper-Symonds equation for rate dependence and typical South African mild steel constants values of 844s-1 for D and 2.207 for q obtained from Hopkinson bar tests [30], a static yield stress of 328MPa is obtained. Quasi-static test data obtained from the tensile test is plotted and shown in Figure 3.

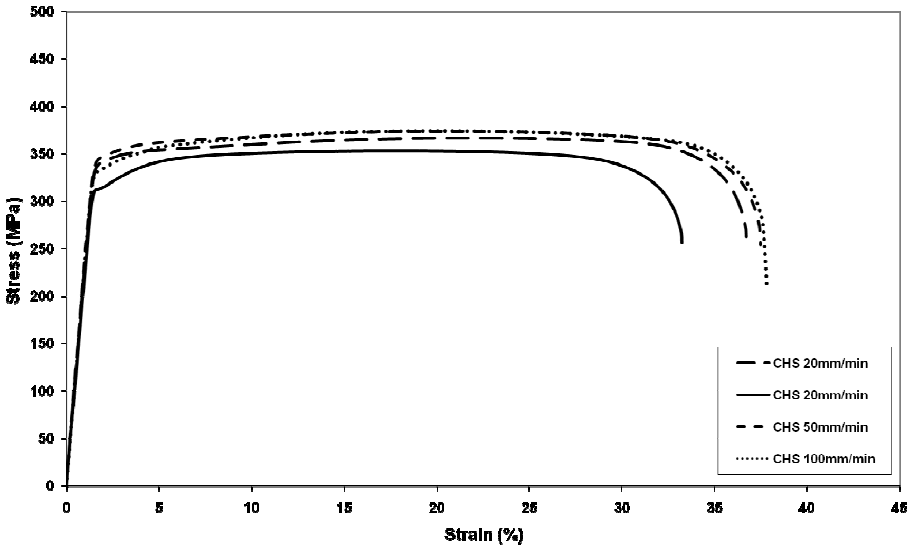

Figure 3 Graph stress vs strain for the tube material.

3 EXPERIMENTAL RESULTS

3.1 Quasi-static axial loading

Quasi-static tests were carried out for three specimen configurations (single tubes, four sides welded tubes and plate-divided tubes) of varying lengths; 400mm, 500mm, 600mm, 700mm, 750mm and 800mm. The results of the quasi-static tests are presented in Table 1. A Zwick testing machine is used to quasi-statically crush the tube specimens in the axial direction. The tubes are crushed at a cross-head speed of 10mm/min. Tests are stopped when a crushed distance of about 73% of the overall length is achieved, close to the stroke efficiency for a crushing tube as defined by Jones [18]. The mean crushing force P_m^s obtained from the Zwick machine is compared with the theoretical values as proposed by Jones [18] in equation (1):

$$P_m^s/M_0 = 52.22\left(C/H\right)^{1/3} \tag{1}$$

where

$$M_0 = \sigma_0 H^2/4 \tag{2}$$

For a 50mm×50mm square tube with a wall thickness of 1.6mm, the theoretical value of P_m^s is 34.53kN. The experimental mean crush force P_m^s is obtained from quasi-static data and calculated by equation (3).

$$P_m^s = \int_0^\delta \frac{F(\delta)}{\delta} d\delta \tag{3}$$

For specimens from 400mm to 700mm, the welded specimens have the lowest P_m^s with an average value for four specimens of 27.69kN. Single tube specimens have an average value for P_m^s of 28.87kN while plate-divided specimens have the highest average value of 29.32kN.

Figures 4-5 illustrate the progressive buckling of quasi-static tests performed on 600mm single, welded and plate-divided specimens, respectively. The labelling letters below each photograph of the crushing progressions in Figure 4-6 correspond to the labelling letters in the axial load-displacement curves shown in Figure 7. In Figures 4 and 5, for the single and welded tubes, the lobe formation is initiated at the bottom of the tube and progresses to the top. For the welded tubes, the weld heat affected zone does not act as a trigger for the buckling process. For the plate divided-specimen, (300p300), shown in Figure 6, the first lobe is formed in the top tube just after the initial ultimate peak load at point (a). Subsequent lobes are formed at points (b)-(e). At point (e) the top tube is crushed to a maximum and another peak load arises as the bottom tube starts to crush. The first lobe is formed in the bottom tube at point (f). Subsequent lobes are formed until the test is stopped at point (j).

Figure 7 shows the axial load–axial displacement graphs and mean crush forces for 600mm single, welded and plate-divided specimens. Ultimate peak forces range from 85kN to 107kN in all specimens. A notable characteristic in all plate-divided specimens is the formation of a second ultimate peak force (see Figure 7) as the second tube starts to buckle after the first tube has crushed to about 80% of its original length. Two ultimate peak loads are undesirable in

Table 1 Results of quasi-static tests.

Specimen	CHS **(mm/min)**	P_m^s **(kN) Actual**	P_{ult} **(kN)**	δ **(mm)**	δ **(%)**	**Buckling mode and number of lobes**
400s	10	28.21	88.90	247	61.25	S (12)
200w200	10	27.48	88.75	290	72.50	S (14)
200p200	10	29.03	86.37	290	72.50	[S (7)] [A (2)-S (5)]
500s	10	28.94	87.45	360	72.00	S (16)
250w250	10	28.18	90.02	360	72.00	S (17)
250p250	10	27.32	85.63	360	72.00	[S (8)] [S (8)]
600s	10	29.12	96.91	435	72.50	S (19)
300w300	10	26.86	92.01	435	72.50	S (19)
300p300	10	31.19	103.16	435	72.50	[S (9)] [S (10)]
700s	10	29.22	96.29	505	72.14	S (23)
350w350	10	28.22	85.17	505	72.14	S (23)
350p350	10	29.72	91.56	505	72.14	[S (10)] [S (12)]
750s	10	30.55	107.81	545	72.67	S (24)
375w375	10	-	89.71	545	72.67	E
375p375	10	-	95.39	545	72.67	E
800s	10	-	108.72	580	72.50	E
400w400	10	-	85.89	580	72.50	E
400p400	10	-	94.69	580	72.50	E

Notation used in table:

A	Asymmetric	( )	Number of complete lobes
E	Global bending	[ ] [ ]	Bottom and top lobe description, respectively
400s	400mm single tube specimen		
200w200	400mm welded tubes specimen		
200p200	400mm plate-divided tubes specimen		

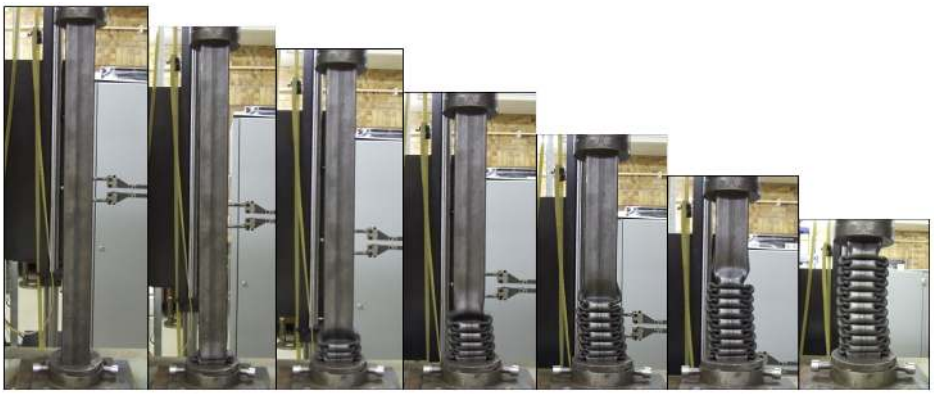

Figure 4 Progressive buckling of single tube specimen 600s.

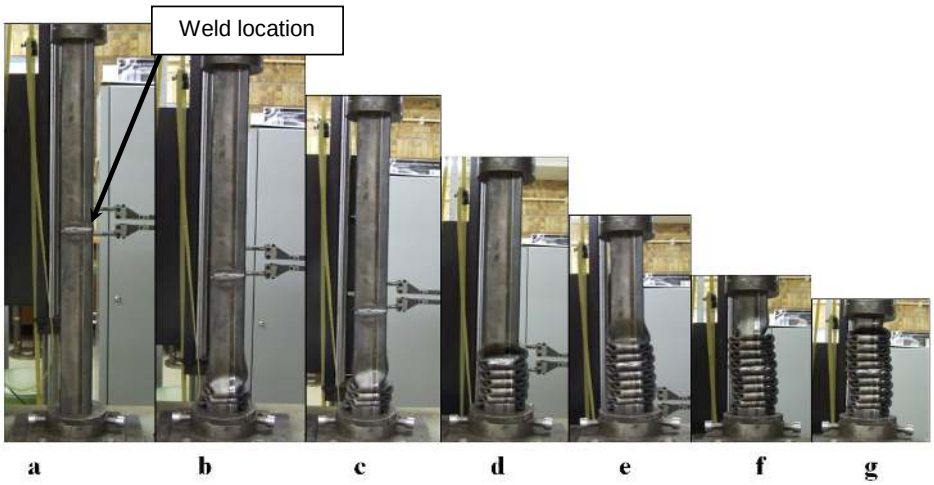

Figure 5 Progressive buckling of welded tubes specimen 300w300.

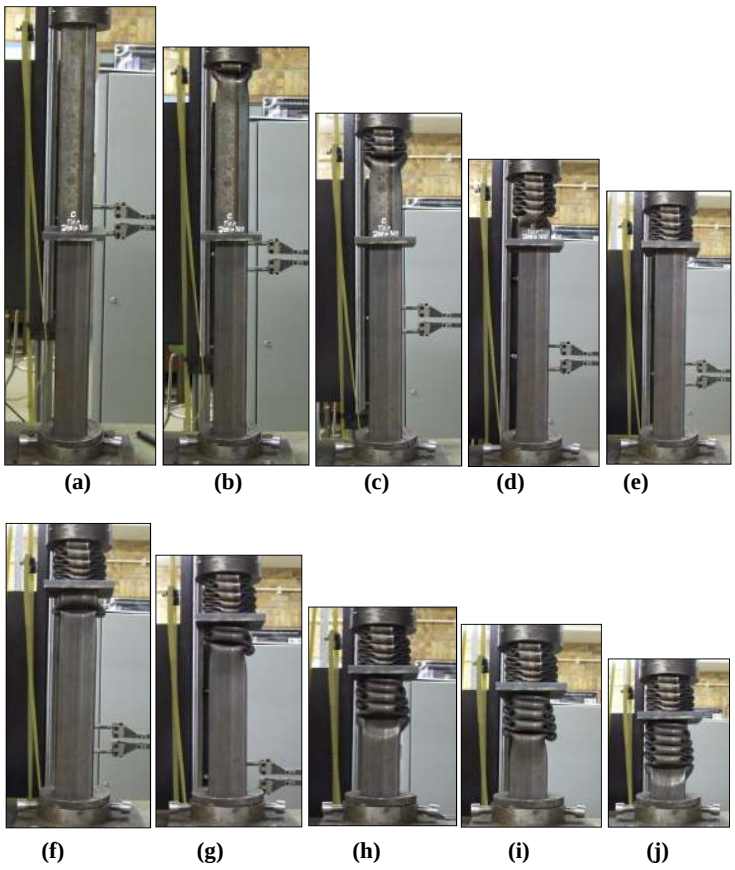

Figure 6 Progressive buckling of plate-divided tubes specimen 300p300.

structural crashworthiness applications since it represents two very large decelerations which in turn pose a great risk to passenger or cargo safety in a vehicle.

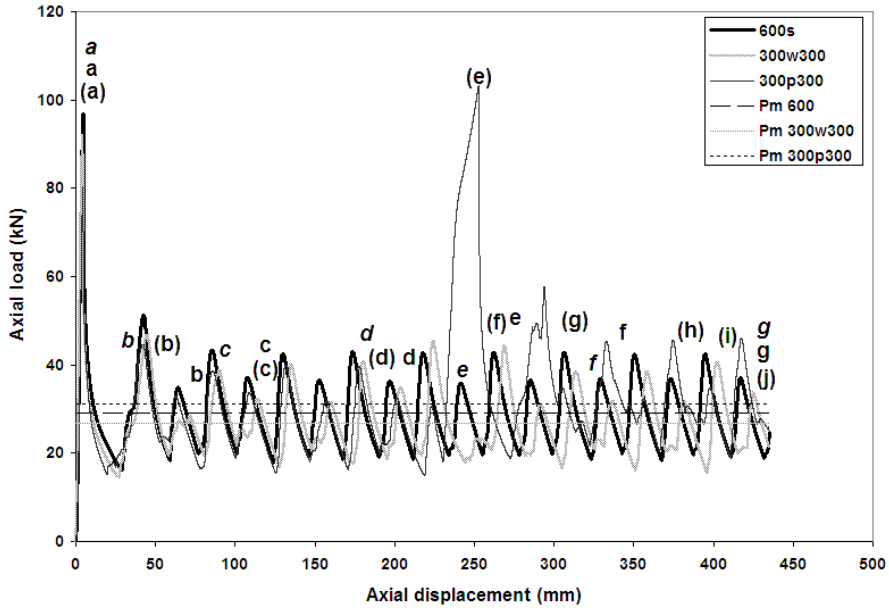

Figure 7 Axial load vs axial displacement graph for 600mm specimens.

The total plastic deformation energy is calculated from the mean crushing force P_m^s and the final cross-head displacement δ.

$$E_{pd} = P_m^s \times \delta \tag{4}$$

A notable characteristic with regard to plate-divided specimens is the initiation of lobe formation. There is no consistency in initial lobe location. Figure 8 shows three of the plate-divided specimens. In 250p250, buckling first occurs at the bottom of the bottom tube followed by the top tube that buckles at the top as shown in Figure 8a. In 300p300, buckling initiates at the top of the top tube followed by the bottom tube buckling from the top as shown in Figure 8b. In 350p350 buckling starts in the top tube at the bottom right above the plate and the bottom tube follows by buckling from the top right below the plate as shown in Figure 8c.

Another feature of axial load-displacement graph of plate-divided specimens is the greater axial displacement required to initiate the second peak load than the first peak load. Figure 9 shows the axial load-displacement curve of 250p250. X1 is the axial displacement of the first crushed tube (in the 250p250 case – bottom tube) required to reach the first peak load of 86kN while X2 is the axial displacement required to reach the second peak load of 80kN which occurs in the second crushed tube (in the 250p250 case – bottom tube). X2 is 12.5mm, almost three times larger that the value of X1 of 4.6mm. As the top tube begins to crush, the bottom tube is still crushed by a small amount. Once lobe formation initiates in the top tube, the bottom tube ceases to displace any further.

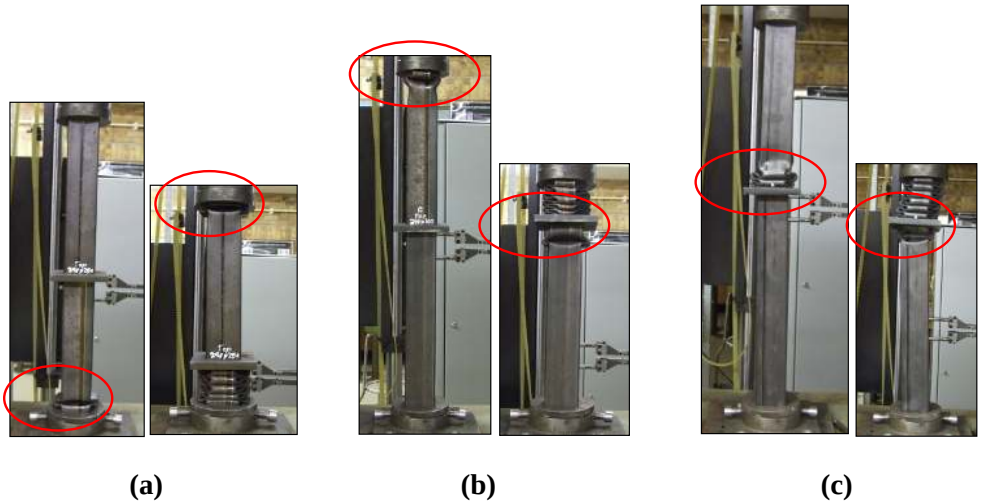

Figure 8 Initiation of lobes in (a) 250p250, (b) 300p300 and (c) 350p350 showing inconsistency in lobe initiation location.

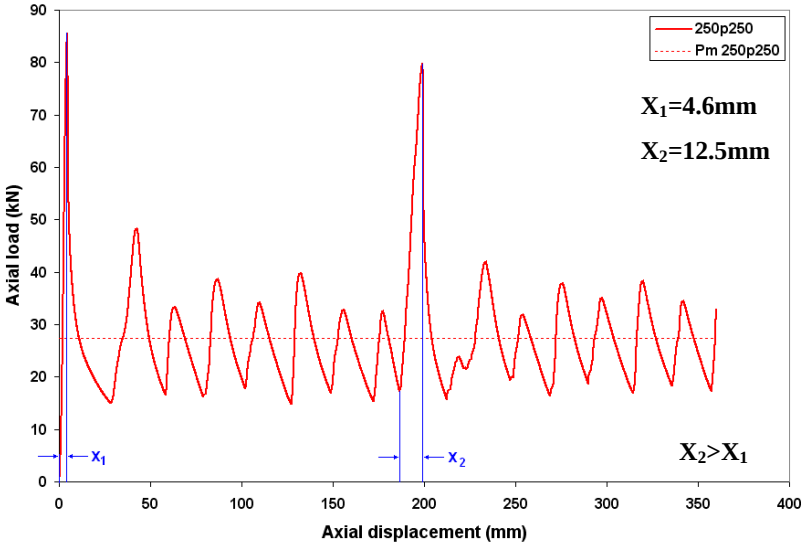

Figure 9 Axial load-displacement graph of specimen 250p250 showing the axial displacement required to reach each peak.

Quasi-static tests revealed a region in which specimens would buckle in the Euler mode instead of the progressive mode. Abramowicz and Jones [3] also noted this behaviour in quasi-static experiments performed on mild steel square tubes. Abramowicz and Jones [3] obtained theoretical and empirical formulae for the critical length-to-width aspect ratio under quasi-static loading and are given by Eq. 5 and 6, respectively:

$$\left(\frac{L}{C}\right)_{cr} = 2\frac{\left(\frac{C}{H}\right)^{1/3}}{1 - 2.88\left(\frac{H}{C}\right)^{4/3}} \qquad \textit{Theoretical} \ [3] \tag{5}$$

and

$$\left(\frac{L}{C}\right)_{cr} = 2.482e^{\left(0.0409\frac{C}{H}\right)} \qquad \textit{Empirical}\,[3] \tag{6}$$

where L and C are the length and width of the tube respectively, and H is the wall thickness of the tube. Eq. 6 was obtained by means of a best fit curve of their experimental data. In Eq. 5 and 6, for tubes with width of C = 50mm and thickness H = 1.6mm, the critical length-to-width aspect ratios are as follows:

$$\left(\frac{L}{C}\right)_{cr} = 6.49 \qquad \textit{Theoretical}\,[3] \tag{7}$$

and

$$\left(\frac{L}{C}\right)_{cr} = 8.91 \qquad \textit{Empirical}\,[3] \tag{8}$$

For single tube specimens, global bending only occurred in the 800mm tube while for welded and plate-divided specimens global bending occurred for 750mm specimens. The 750mm single tube specimen 750s buckled in a progressive manner. Figure 10 shows how results of quasi-static tests compared to the theoretical and empirical curves obtained by Abramowicz and Jones [3].

From the theoretical equation (see Eq. 5), Abramowicz and Jones [3] predicted that global bending would occur at a critical length-to-width aspect ratio of 6.49. The experimental data yielded an increase of this ratio to 8.91 (Eq. 8). Table 2 shows the critical length-to-width aspect ratio of the quasi-static tests. From the current results it appears that for single tubes the critical ratio lies between 15 and 16 while for welded and plate-divided specimens the critical ratio is between 14 and 15.

3.2 Dynamic axial loading

The test rig used for the dynamic impact loading is a 7m high drop tester. The specimen is securely clamped to the anvil of the rig. In plate-divided specimens, the rigid square plate (as used for the quasi-static test) is placed on top of the bottom tube with the top tube placed on top of it. Care is taken to ensure that each specimen is level so that it is likely to crush in the desired manner. The drop mass is kept constant at 340 kg. The drop heights used and their corresponding impact velocities are shown in Table 3. The drop tester is not equipped with data acquisition equipment and hence no force-displacement histories are recorded for analysis.

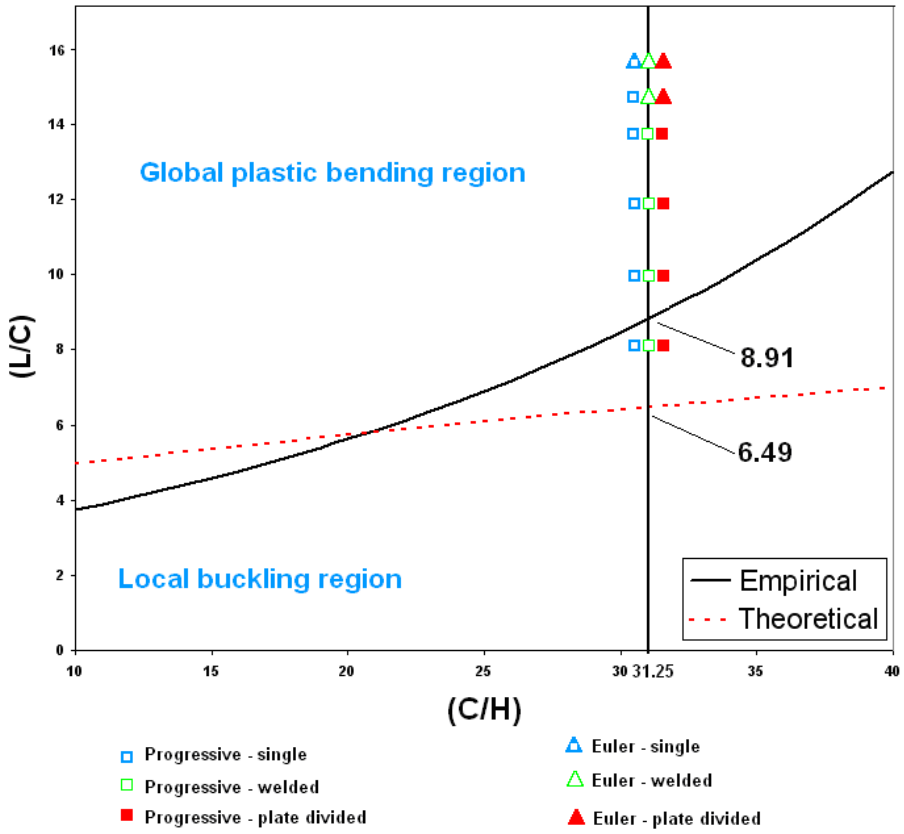

Figure 10 Length-to-width ratio versus width-to-thickness ratio graph showing quasi-static data (C/H = 31.25) compared to lines separating global plastic bending (Euler buckling) and local buckling (progressive buckling) obtained by Abramowicz and Jones [3].

Applying the conservation of energy equations assuming no losses due to friction, the total plastic deformation energy E_{pd} that is the energy absorbed by a single and welded specimen is given by

$$E_{pd} = Mg\,(h + \delta) \tag{9}$$

where δ is the crushed distance of the specimen. For plate-divided specimens the total crushed distance is the summation of the crushed distance of the top and bottom tubes (Eq. 10).

$$\delta = \delta_{bottom} + \delta_{top} \tag{10}$$

where δ_{bottom} and δ_{top} are the axial displacements of the bottom and top tubes respectively.

The mean dynamic crushing force Pdm is calculated from the total energy absorbed and the displacement of a specimen.

$$P_m^d = {}^{E_{pd}}/_{\delta} \tag{11}$$

Table 2 Length-to-width aspect ratios of quasi-static specimens.

Specimen	L *(mm)*	C *(mm)*	H *(mm)*	$\left(\frac{L}{C}\right)$	$\left(\frac{L_{bottom}}{C}\right)$	$\left(\frac{L_{top}}{C}\right)$	$\left(\frac{C}{H}\right)$	*Buckling mode and number of lobes*
400s	400	50	1.6	8	-	-	31.25	S (12)
200w200	400	50	1.6	8	-	-	31.25	S (14)
200p200	400	50	1.6	8	4	4	31.25	[S (7)] [A (2)-S (5)]
500s	500	50	1.6	10	-	-	31.25	S (16)
250w250	500	50	1.6	10	-	-	31.25	S (17)
250p250	500	50	1.6	10	5	5	31.25	[S (8)] [S (8)]
600s	600	50	1.6	12	-	-	31.25	S (19)
300w300	600	50	1.6	12	-	-	31.25	S (19)
300p300	600	50	1.6	12	6	6	31.25	[S (9)] [S (10)]
700s	700	50	1.6	14	-	-	31.25	S (23)
350w350	700	50	1.6	14	-	-	31.25	S (23)
350p350	700	50	1.6	14	7	7	31.25	[S (10)] [S (12)]
750s	750	50	1.6	15	-	-	31.25	S (24)
375w375	750	50	1.6	15	-	-	31.25	E
375p375	750	50	1.6	15	7.5	7.5	31.25	E
800s	800	50	1.6	16	-	-	31.25	E
400w400	800	50	1.6	16	-	-	31.25	E
400p400	800	50	1.6	16	8	8	31.25	E

Notation used in table:

A	Asymmetric	( )	Number of complete lobes
E	Global bending	[ ] [ ]	Bottom and top lobe description, respectively
400s	400mm single tube specimen		
200w200	400mm welded tubes specimen		
200p200	400mm plate-divided tubes specimen		

where δ is the crushed distance. This is compared to the theoretical mean dynamic crushing force given by Jones [18] as

$$P^d_{m(theoretical)} = 13.05\sigma_o H^2 \left(C/H\right)^{1/3} \left\{1 + \left(\frac{0.33V_o}{CD}\right)^{1/q}\right\} \tag{12}$$

Using Eq. 12, the theoretical values for the mean dynamic crushing force are calculated. The mean dynamic crushing forces for the different drop heights, calculated using Eq. 12 and shown in Table 3, under predict the mean dynamic crushing force obtained from Eq. 11, shown in Tables 4-7.

Dynamic test results are summarized in Tables 4-7. **Group A** refers to tests performed on plate-divided specimens ranging from 250 to 450mm in length and are presented in Table 4. **Group B** refers to preliminary tests performed on axially welded tubes with different weld configurations and are presented in Table 5. **Group C** refers to tests performed on single and

Table 3 Theoretical mean dynamic crushing forces for given drop heights.

Drop Height (m)	Impact Velocity of Drop Mass (m/s)	P_m^d (kN) (theoretical)
1.69	5.75	41.94
2.15	6.50	42.40
2.68	7.25	42.85
3.26	8.00	43.26
3.90	8.75	43.66

welded specimens ranging from 300mm to 500mm and are presented in Table 6. **Group D** refers to tests performed on single, welded and plate-divided specimens ranging from 550mm to 1700mm in length and are presented in Tables 7. Figures 11-12 show the buckling modes and crushed tubes of all tests performed at a drop height of 3.26m for all the different groups.

Table 4 Experimental data for Group A dynamic tests (plate-divided specimens (with C = 50mm, H = 1.6mm and M = 340kg).

Specimen	L **(mm)**	h **(m)**	V **(m/s)**	δ_{L1} **(mm)**	δ_{L2} **(mm)**	δ_{total} **(mm)**	E_{pd} **(kJ)**	P_m^d **(kN)**	**Deformation mode [lobes]**
150p100A	250	3.293	8.04	92.1	82.6	175	11.57	66.20	IF [3.5][2]
150p100B	250	2.148	6.49	-	-	-	-	-	TS
150p100C	250	2.153	6.50	80.2	82.8	163	7.72	47.40	S [3][2.5]
150p125A	275	2.152	6.50	54.4	103.3	158	7.70	48.85	S [2][4]
150p125B	275	2.676	7.25	-	-	-	-	-	FO
150p125C	275	2.683	7.26	56.0	104.5	161	9.48	59.08	S [1.5][3.5]
150p125D	275	3.291	8.04	110.3	103.4	214	11.69	54.69	S [4.5][4.5]
150p150A	300	3.286	8.03	94.4	116.4	211	11.66	55.33	S [3.5][5]
150p150B	300	2.681	7.25	-	-	-	-	-	FO
150p150C	300	2.155	6.50	23.2	121.0	144	7.67	53.18	S [1][4.5]
100p200A	300	3.262	8.00	37.9	163.1	201	11.55	57.46	S [1][7]
100p200B	300	2.682	7.25	7.3	161.6	169	9.51	56.31	S [0.5][6.5]
100p200C	300	2.155	6.50	79.2	55.5	135	7.64	56.76	IF [2.5][1.5]
100p200D	300	2.159	6.51	0.0	134.3	134	7.65	56.94	S [0][5.5]
150p175A	325	3.287	8.03	70.1	138.8	209	11.66	55.81	S[3.5][5.5]
150p175B	325	2.682	7.25	-	-	-	-	-	FO
150p175C	325	2.682	7.25	23.6	142.9	167	9.50	57.06	S [1][5.5]
150p175D	325	2.161	6.51	0.0	141.0	141	7.68	54.47	IF [0][6]
125p200A	325	3.258	8.00	36.7	157.6	194	11.51	59.27	S [1][7]
125p200B	325	2.679	7.25	8.1	165	173	9.51	54.95	S [0.5][6.5]
125p200C	325	2.152	6.50	0.0	148.7	149	7.67	51.59	S [0][6]

Table 4 Experimental data for Group A dynamic tests (plate-divided specimens (with C = 50mm, H = 1.6mm and M = 340kg) *(continued)*.

Specimen	L **(mm)**	h **(m)**	V **(m/s)**	δ_{L1} **(mm)**	δ_{L2} **(mm)**	δ_{total} **(mm)**	E_{pd} **(kJ)**	P_m^d **(kN)**	**Deformation mode [lobes]**
150p200A	350	3.260	8.00	-	-	-	-	-	Fo
150p200B	350	3.258	8.00	34.1	163.3	197	11.53	58.38	S [1][6.5]
150p200C	350	3.298	8.04	38.1	158.9	197	11.66	59.19	S [1][6]
150p200D	350	2.681	7.25	22.5	160.8	183	9.55	52.12	S [1][6.5]
150p200E	350	2.684	7.26	5.3	161.6	167	9.51	57.00	S [0.5][6.5]
150p200F	350	2.154	6.50	0.0	131.1	131	7.62	58.12	If [0][6.5]
150p200G	350	2.150	6.49	-	-	-	-	-	FO
150p200H	350	2.152	6.50	-	-	-	-	-	FO
150p200I	350	2.156	6.50	0.0	155.2	155	7.71	49.66	S [0][6.5]
175p200A	375	3.897	8.75	55.7	165.0	221	13.76	62.23	IF [1.5][6]
175p200B	375	3.288	8.03	-	-	-	-	-	Fo
175p200C	375	3.266	8.00	30.5	164.9	195	11.55	59.07	S [1][6.5]
175p200D	375	2.682	7.25	0.0	161.7	162	9.48	58.66	S [0][6.5]
200p200A	400	3.901	8.75	-	-	-	-	-	FO
200p200B	400	3.288	8.03	-	-	-	-	-	FO
200p200C	400	3.258	8.00	18.3	160.5	179	11.46	64.10	IF [1][4]
225p200A	425	4.313	9.20	55.5	165.7	221	15.12	68.37	S [1.5][5.5]
225p200B	425	3.901	8.75	65.9	162.4	228	13.77	60.32	S [2.5][6.5]
225p200C	425	3.292	8.04	28.8	164.2	193	11.62	60.19	IF [1][6]
225p200D	425	2.682	7.25	0.0	160.3	160	9.48	59.15	IF [0][5]
225p200E	425	2.125	6.46	-	-	-	-	-	FO
250p200A	450	3.902	8.75	-	-	-	-	-	FO
250p200B	450	3.917	8.77	194.2	34.6	229	13.83	60.42	S [8][1]
250p200C	450	3.292	8.04	42.8	162.2	205	11.66	56.90	S [1][7]
250p200D	450	2.676	7.25	0.0	164.4	164	9.47	57.76	S [0][6]

Notation used in table:

p	plate-divided tubes specimen	S	Symmetric progressive
A	Asymmetric progressive	T	Transition
E	Global bending	TS	Tearing and splitting
FO	Fly-out failure	[ ] [ ]	Number of complete lobes in bottom and top tube, respectively
IF	Irregular folding		

Table 5 Experimental data for Group B dynamic tests (different weld configurations) (with C = 50mm, H = 1.5mm and M = 340kg).

Specimen	Weld type	L_{bottom} (mm)	L_{top} (mm)	h (m)	V (m/s)	δ_{total} (mm)	E_{pd} (kJ)	P_m^d (kN)	Deformation mode [lobes]
A1a		150	200	3.260	8.00	231	11.64	50.51	S [11]
A1b		150	200	3.260	8.00	-		-	WF – TS
A1c		150	200	3.259	8.00	272	11.78	43.23	A [11]
A1d		150	200	3.259	8.00	262	11.74	44.90	S [11]
A2a		150	200	3.900	8.75	296	13.99	47.36	S [12]
A2b		150	200	3.259	8.00	-	-	-	WF – TS
A2c		150	200	3.603	8.40	-	-	-	WF – TS
A2d		150	200	3.594	8.40	-	-	-	WF – TS
A3b		150	200	3.260	8.00	-	-	-	WF – TS
A3c		150	200	3.596	8.40	286	12.95	45.32	S[11]
A3d		150	200	3.603	8.40	286	12.97	45.31	S [10]
B1a		200	200	3.259	8.00	286	11.82	41.31	S [12]
B1b		200	200	3.259	8.00	300	11.87	39.58	S [12]
B1c		200	200	3.259	8.00	253	11.71	46.27	A [10]
B1d		200	200	3.260	8.00	273	11.79	43.12	S [12]
B2a		200	200	3.596	8.40	318	13.06	41.00	S [13]
B2b		200	200	3.597	8.40	321	13.07	40.73	S [13]
B2c		200	200	3.601	8.40	316	13.07	41.30	S [13]
B2d		200	200	3.596	8.40	318	13.05	41.07	S [12]
C1a		250	200	3.263	8.00	284	11.83	41.63	A [12]
C1b		250	200	3.256	8.00	292	11.83	40.51	S [12]
C1c		250	200	3.264	8.00	298	11.88	39.83	S[12]
C1d		250	200	3.259	8.00	-	-	-	E
C2c		250	200	3.598	8.40	347	13.16	37.88	S [15]
C3a		250	200	3.596	8.40	336	13.11	39.04	S [15]
C3b		250	200	3.599	8.40	326	13.09	40.19	S [15]
C3c		250	200	3.598	8.40	-	-	-	WF – TS
C3d		250	200	3.599	8.40	-	-	-	WF - TS

Notation used in table:

A	Asymmetric progressive	T	Transition	c	side spot welds
E	Global bending	TS	Tearing and shearing	d	two-sided seam-weld
IF	Irregular folding	a	four-sided seam-weld	WF	Weld failure
S	Symmetric progressive	b	corner spot welds	[ ]	Number of complete lobes in bottom and top tube, respectively

	4-sided seam	Corner spots	Side spots	2-sided seams
Weld schematic		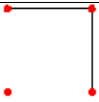		

Table 6 Experimental data for Group C dynamic tests on single and welded square tubes (with C = 50mm, H = 1.6mm and M = 340kg).

Specimen	**L (mm)**	**h (m)**	**V (m/s)**	δ_{total} **(mm)**	E_{pd} **(kJ)**	P_m^d **(kN)**	**Deformation mode [lobes]**
300sA	300	3.257	7.99	255	11.71	45.97	S [10]
150w150A	300	3.258	8.00	250	11.70	46.86	S [11]
300sB	300	2.679	7.25	238	9.73	40.81	S [10]
150w150B	300	2.679	7.25	227	9.69	42.77	S [10]
300sC	300	2.148	6.49	190	7.80	40.96	S [7]
150w150C	300	2.149	6.49	166	7.72	46.57	A [7]
300sD	300	1.689	5.76	145	6.12	42.24	S [5.5]
150w150D	300	1.688	5.75	124	6.05	48.60	a [5.5]
400sA	400	3.903	8.75	323	14.10	43.61	s [13]
200w200A	400	3.901	8.75	318	14.07	44.23	s [14]
400sB	400	3.263	8.00	285	11.83	41.58	s [11.5]
200w200B	400	3.260	8.00	269	11.77	43.70	s [12.5]
400sC	400	2.680	7.25	229	9.70	42.41	s [9.5]
200w200C	400	2.680	7.25	225	9.69	43.02	s [9.5]
400sD	400	2.150	6.49	192	7.81	40.68	s [7.5]
200w200D	400	2.150	6.49	182	7.78	42.70	s [7.5]
500sA	500	3.263	8.00	292	11.86	40.63	s [12]
250w250A	500	3.260	8.00	289	11.84	40.93	s [12.5]
500sB	500	2.682	7.25	235	9.73	41.35	s [9.5]
250w250B	500	2.680	7.25	226	9.69	42.85	s[9.5]
500sC	500	2.153	6.50	184	7.79	42.45	s [7]
250w250C	500	2.150	6.49	161	7.71	47.84	s [7]
500sD	500	2.153	6.50	165	7.73	46.73	s [7]
250w250D	500	2.149	6.49	165	7.72	46.83	s [7]
550s	550	3.258	8.00	178	11.46	64.38	S [8.5]
275w275A	550	3.259	8.00	-	-	-	T [4.5]
275w275B	550	3.259	8.00	200	11.54	57.69	A [1] - S [7]
275p275	550	3.261	8.00	200	11.54	57.72	S [0][7.5]
600sA	600	3.260	8.00	-	-	-	T [6]
600sB	600	3.258	8.00	156	11.39	72.99	IF [7]
300w300A	600	3.263	8.00	192	11.52	60.02	S [7.5] - T
300w300B	600	3.260	8.00	187	11.50	61.48	S [8.5]
300p300	600	3.258	8.00	190	11.50	60.53	S [0][8.5]
650sA	650	3.257	7.99	-	-	-	T [6]
650sB	650	3.257	7.99	185	11.48	62.06	S [7.5]
325w325	650	3.261	8.00	180	11.48	63.76	IF [5]
325p325A	650	3.258	8.00	168	11.43	68.02	IF [0][8] - T
325p325B	650	3.260	8.00	182	11.48	63.08	A [0][8.5]
700s	700	3.263	8.00	185	11.50	62.16	S [7.5]

Table 6 Experimental data for Group C dynamic tests on single and welded square tubes (with C = 50mm, H = 1.6mm and M = 340kg) *(continued)*.

Specimen	**L (mm)**	**h (m)**	**V (m/s)**	δ_{total} **(mm)**	E_{pd} **(kJ)**	P_m^d **(kN)**	**Deformation mode [lobes]**
350w350	700	3.260	8.00	-	-	-	T [4]
350p350	700	3.257	7.99	138	11.32	82.06	S [7.5][0] - T
800sA	800	3.260	8.00	185	11.49	62.08	S [7.5]
800sB	800	3.260	8.00	186	11.49	61.79	IF [7.5]
400w400	800	3.260	8.00	207	11.56	55.86	IF [7.5]
400p400	800	3.261	8.00	197	11.53	58.60	S [0][7.5]
900s	900	3.260	8.00	202	11.55	57.16	S [7.5]
450w450	900	3.260	8.00	216	11.59	53.68	s [8.5]

Notation used in table:

A	Asymmetric progressive	T	Transition
E	Global bending	[ ][ ]	Number of complete lobes in bottom and top tube, respectively
FO	Fly-out failure	300s	300mm single tube specimen
IF	Irregular folding	150w150	300mm welded tubes specimen
S	Symmetric progressive		

Table 7 Experimental data for Group D dynamic tests performed on single, welded and plate-divided square tubes (with C = 50mm, H = 1.6mm and M = 340kg).

Specimen	**L (mm)**	**h (m)**	**V (m/s)**	δ_{total} **(mm)**	E_{pd} **(kJ)**	P_m^d **(kN)**	**Deformation mode [lobes]**
550s	550	3.258	8.00	178	11.46	64.38	S [8.5]
275w275A	550	3.259	8.00	-	-	-	T [4.5]
275w275B	550	3.259	8.00	200	11.54	57.69	A [1] - S [7]
275p275	550	3.261	8.00	200	11.54	57.72	S [0][7.5]
600sA	600	3.260	8.00	-	-	-	T [6]
600sB	600	3.258	8.00	156	11.39	72.99	IF [7]
300w300A	600	3.263	8.00	192	11.52	60.02	S [7.5] - T
300w300B	600	3.260	8.00	187	11.50	61.48	S [8.5]
300p300	600	3.258	8.00	190	11.50	60.53	S [0][8.5]
650sA	650	3.257	7.99	-	-	-	T [6]
650sB	650	3.257	7.99	185	11.48	62.06	S [7.5]
325w325	650	3.261	8.00	180	11.48	63.76	IF [5]
325p325A	650	3.258	8.00	168	11.43	68.02	IF [0][8] - T
325p325B	650	3.260	8.00	182	11.48	63.08	A [0][8.5]
700s	700	3.263	8.00	185	11.50	62.16	S [7.5]
350w350	700	3.260	8.00	-	-	-	T [4]
350p350	700	3.257	7.99	138	11.32	82.06	S [7.5][0] - T
800sA	800	3.260	8.00	185	11.49	62.08	S [7.5]
800sB	800	3.260	8.00	186	11.49	61.79	IF [7.5]

Table 7 Experimental data for Group D dynamic tests performed on single, welded and plate-divided square tubes (with C = 50mm, H = 1.6mm and M = 340kg) *(continued)*.

Specimen	**L (mm)**	**h (m)**	**V (m/s)**	δ_{total} **(mm)**	E_{pd} **(kJ)**	P_m^d **(kN)**	**Deformation mode [lobes]**
400w400	800	3.260	8.00	207	11.56	55.86	IF [7.5]
400p400	800	3.261	8.00	197	11.53	58.60	S [0][7.5]
900s	900	3.260	8.00	202	11.55	57.16	S [7.5]
450w450	900	3.260	8.00	216	11.59	53.68	s [8.5]
1000s	1000	3.263	8.00	175	11.47	65.57	A [0][7]
500w500	1000	3.262	8.00	178	11.47	64.46	IF [8] - T
500p500	1000	3.260	8.00	201	11.54	57.51	S [0][8]
1100s	1100	3.260	8.00	-	-	-	T [6]
550w550	1100	3.261	8.00	215	11.59	53.92	S [8.5]
550p550	1100	3.257	7.99	218	11.59	53.17	S [0][8.5]
1200sA	1200	3.258	8.00	137	11.32	82.74	IF [6]
1200sB	1200	3.257	7.99	190	11.50	60.51	IF [7.5]
600w600	1200	3.258	8.00	-	-	-	T [6]
600p600	1200	3.258	8.00	174	11.45	65.92	S [0][7.5]
1300s	1300	3.258	8.00	207	11.56	55.83	S [8]
650w650	1300	3.262	8.00	206	11.57	56.15	S [8]
650p650	1300	3.258	8.00	212	11.57	54.59	s [0][8]
1400s	1400	3.260	8.00	185	11.49	62.11	IF [7]
700w700	1400	3.258	8.00	185	11.48	62.07	IF [7]
700p700	1400	3.258	8.00	193	11.51	59.64	If [0][7]
1500s	1500	3.259	8.00	205	11.55	56.36	S [7.5]
750w750A	1500	3.259	8.00	-	-	-	T [4]
750w750B	1500	3.263	8.00	170	11.45	67.36	S [6.5] - T
750p750A	1500	3.258	8.00	196	11.52	58.78	S [0][7.5] - FO
750p750B	1500	3.263	8.00	178	11.48	64.48	S [0][7.5]
1600s	1600	3.262	8.00	197	11.54	58.56	S [7.5]
800w800	1600	3.261	8.00	-	-	-	E
800p800	1600	3.260	8.00	163	11.42	70.04	S [0][8] - FO
1700s	1700	3.260	8.00	190	11.51	60.56	S [7.5] - T
850w850	1700	3.259	8.00	215	11.59	53.89	S [8.5]
850p850	1700	3.260	8.00	201	11.54	57.43	S [0][8.5]

Notation used in table:

A	Asymmetric progressive	T	Transition
E	Global bending	[ ][ ]	Number of complete lobes in bottom and top tube, respectively
FO	Fly-out failure	500s	500mm single tube specimen
IF	Irregular folding	250w250	500mm welded tubes specimen
S	Symmetric progressive	250p250	500mm plate-divided tubes specimen

In Group A, 46 dynamic tests were performed on plate-divided specimens; 34 of which provided successful results and 12 unsuccessful or failed tests which included bending, splitting and tearing. The lengths of the specimens were in the progressive buckling region ranging from 250mm to 450mm. Figure 11 shows original and crushed profiles of some specimens tested with a drop height of 3.26m. The bottom tube length was kept constant while the top tube length was increased incrementally in 25mm steps from 100mm to 200mm. In each case, as the top tube was crushed to a maximum, the energy would be transferred through the rigid plate and the lobe formation would continue in the bottom tube. The buckling progress in the bottom tube appears to randomly initiate either at the top or bottom end of the bottom tube.



Figure 11 Plate-divided specimens with $L_{bottom} = 150$mm and L_{top} ranging from 100mm to 200mm in 25mm increments. h = 3.26m.

In Group B, different weld configurations were tested (see Figure 1). Of these 28 tests, 20 provided successful results while 8 yielded unsuccessful results. The welded specimens were within the progressive buckling region with original lengths of 350mm, 400mm and 450mm and were labelled Series A, B and C for these lengths, respectively. The wall thicknesses of these specimens were 1.5mm instead of 1.6mm as in other groups. Four different weld configurations were tested. These included four-sided seam weld, corner spot welds, side spot welds and two sided seam welds. Most specimens buckled progressively while other specimens deformed due to bending, splitting or tearing. Table 8 shows schematic diagrams of the weld configurations and summarises the test results in terms of number of successful and failed tests. Table 8 indicates that the four-sided seam welded specimens are the most reliable as all the tests performed on these types of specimens provided desirable results. Of the welded specimens, the corner spot welded and two-sided seam welded specimens were the least reliable, with each configuration only yielding four out of seven useful results. Two drop heights, 3.26m and 3.6m, were used. These drop heights correspond to impact velocities of 8m/s and 8.4m/s respectively. Figure 12 shows original lengths and crushed profiles of 400mm specimens tested at a drop height of 3.6m. Results for these tests are tabulated in Table 9. From Figure 12 and the results in Table 9, it is clear that the weld type makes very little difference to the deformation mode and efficiency in terms of crushed distance in a welded tube. There is

only a 5mm difference in crushed distance between the four different specimens. High-speed camera footage was obtained for these four welded specimens (Progressive buckling sequence for specimen B2a obtained from high speed camera footage is shown in Figure 13, the weld heat affected zone does not act as a trigger for the buckling process.). The time taken to stop the drop mass is approximately the same in each specimen (70ms). This in turn indicates that the average deceleration of the impact mass is the same in each specimen. All four specimens decelerated the drop mass by about 110m/s^2.

Table 8 Successful and failed results summary of welded tube specimens.

	4-sided seam	Corner spots	Side spots	2-sided seams	Total
Weld schematic	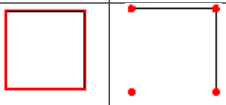				
Progressive buckling	6	4	6	4	20
Irregular buckling, tearing and splitting	0	3	2	3	8

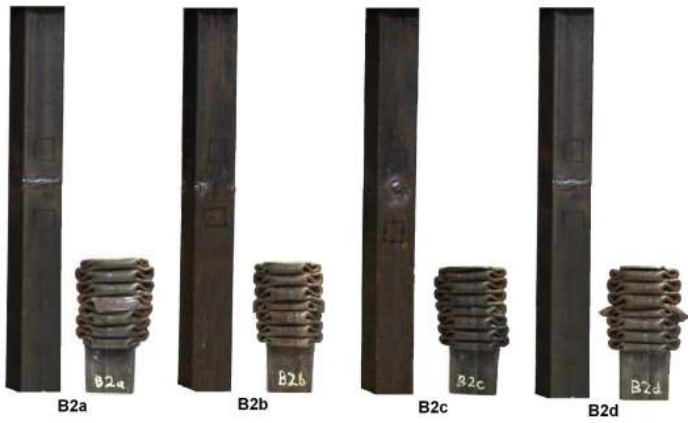

Figure 12 400mm specimens tested with h = 3.60m.

In Group C single and seam-welded tubes with lengths of 300mm, 400mm and 500mm were tested. 24 tests were performed; 12 on single tube specimens and 12 on welded specimens. Specimens were tested at drop heights of 3.26m, 2.68m, 2.15m and 1.69m. The welded specimens consisted of two tubes welded together at their ends such that the weld was half

Table 9 Results of tests performed on 400mm welded specimens with h = 3.60m.

Specimen	Weld type	L1 (mm)	L2 (mm)	δ_t (mm)	E_{pd} (kJ)	P_m^d (kN)
B2a		200	200	318	13.06	41.00
B2b	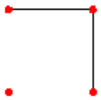	200	200	321	13.07	40.73
B2c	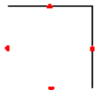	200	200	316	13.07	41.30
B2d	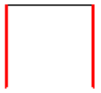	200	200	317	13.05	41.07

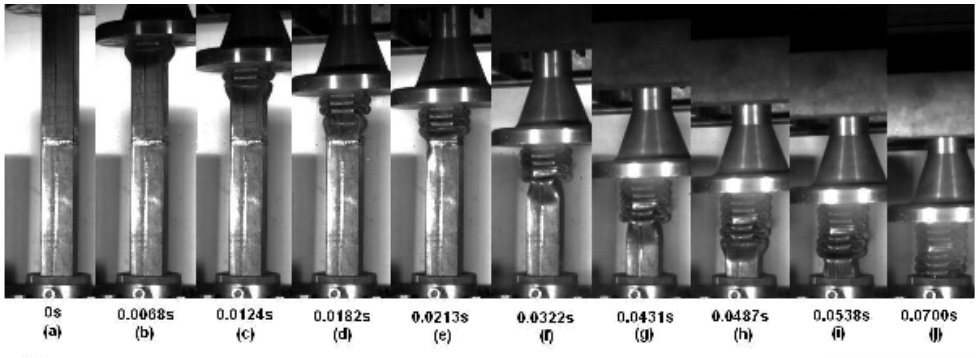

Figure 13 Progressive buckling sequence for specimen B2a obtained from high speed camera footage.

way along the specimen (not including the 50mm allowed for clamping). Table 6 shows that single tubes crushed more than welded equivalents in all tests performed in this group but not by a large amount. The maximum difference in crushed distance between single and welded specimens is 24 mm between 300sC and 150w150C while the smallest difference was 0mm between 500sD and 250w250D. The seam-weld did not inhibit lobe formation but caused the specimens to crush less than their single tube equivalents because the lobe that formed over the weld in each case used slightly more material to form, thus resisting crushing.

In Group D single, welded and plate-divided specimens with lengths ranging from 550mm to 1700mm were tested. Every test was performed at a drop height of 3.26m corresponding to an impact velocity of 8m/s. Of these 50 tests, 7 of the specimens buckled in the transition

mode (characterised by progressive buckling and ultimately global bending) while only one specimen experienced global bending. Most specimens buckled progressively in a symmetric manner while others, although deformed progressively, could be seen to be on the verge of the transition region. Although transition buckling was not observed in quasi-static tests, it was certainly seen in dynamic tests. This behaviour is consistent with the experimental observations of Abramowicz and Jones [3]. Eq 13 and 14 refer to empirical formulae obtained by Abramowicz and Jones [3] for the critical lengths under dynamic loading and are given by

$$\left(\frac{L}{C}\right)_{cr} = 2.453e^{(0.08\frac{C}{H})} \qquad Empirical[3] \tag{13}$$

and

$$\left(\frac{L}{C}\right)_{cr} = 3.423e^{(0.04\frac{C}{H})} \qquad Empirical[3] \tag{14}$$

The chart, plotted in Figure 14, summarizes the experimental data and shows a scatter of crushed distances for the different tube configurations. No obvious trends are present. The four horizontal lines running parallel with the abscissa indicate the modes of collapse observed at the various discrete specimen lengths along this axis. It should be noted that for some specimens, for example at a length of 1600mm the crushed distance of the two specimens exhibiting transition buckling and Euler buckling, the crushed distance was not measured and hence not included in the graph.

Abramowicz and Jones [3] found that in general the transition from progressive to global buckling for a given thickness, the critical length-to-width ratio given by the value $(L/C)_{cr}$ was larger under dynamic loading than for quasi-static loading. Results confirmed this tendency as only one specimen (1600mm welded specimen 800w800) in the entire test matrix exhibited purely global bending. This welded specimen has a $(L/C)_{cr}$ of 32 while in quasi-static tests welded specimen displayed global buckling at a ratio $(L/C)_{cr}$ of 15. Purely global bending did not occur in single and plate-divided specimens. Figure 15 is a length-to-width versus width-to thickness chart plotting all data points from **Group A, B, C** and **D**. These points are compared with Eqs. 13 and 14 obtained by Jones.

Plate-divided specimens did not exhibit any transition or global bending. In most cases, specimens buckled progressively in a symmetric manner. Transition and global bending are undesirable collapse modes in tubular structures and are not favourable to plastic deformation energy absorption. At some specimen lengths, while single or welded tubes buckled in a transition or global bending manner, plate-divided specimens would buckle progressively. Figure 16 illustrates this occurrence in the form of 1100mm specimens. The 1100mm single tube crushed in a transition manner while the 1100mm welded and plate-divided specimen crushed in a progressive manner. In other cases where all three specimen configurations buckled in the progressive mode, the plate-divided specimen would crush more than the single and welded tube configurations. This behaviour was noticed in longer tube specimens but in shorter tube specimens, the plate-divided specimens would crush less than the welded and single tubes. In some plate-divided specimens, *fly-out failures* occurred. *Fly-out failure* was a term coined in

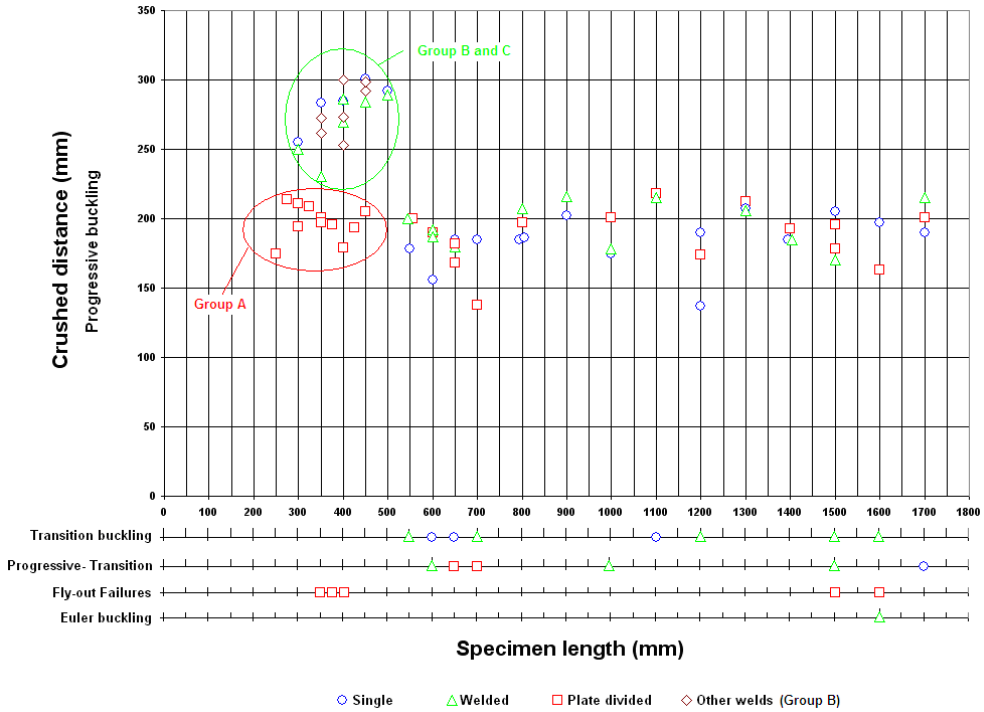

Figure 14 Crushed distances and buckling mode chart of dynamic tests performed with h = 3.26m (V_o = 8m/s).

tests performed on specimens in **Group A** where it was often observed that as a plate-divided specimen was struck by the drop mass, the top tube and plate would slip out leaving the clamped bottom tube alone to be crushed by the mass as it continued to fall. It should be noted that the plate and top tube were only balanced loosely and not tied to each other in any way. Fly-out failures were common in plate-divided specimens up to 400mm in length but were observed in 1500mm and 1600mm specimens at impact velocities of 8m/s. At lower impact velocities (5.75m/s, 6.5m/s and 7.25m/s), fly-out failures were most prevalent.

4 DISCUSSION OF RESULTS

4.1 Static behaviour

Single, welded and plate-divided specimens with lengths ranging from 400mm to 800mm were quasi-statically axially loaded. The tubes all had width-to-thickness ratios (C/H) of 31.25. For this width-to-thickness ratio Abramowicz and Jones [3] predicted that buckling would change from progressive to global bending in single tubes at a critical length-to-width aspect ratio (L/C) of 6.49. The experimental data yielded an increase of this ratio to 8.91. Results showed that for single tubes global bending first occurred in single tubes at 800mm (critical length-to-width aspect ratio of 16). For welded and plate-divided tube specimens, global bending occurred at 750mm (critical length-to-width aspect ratio of 15). No transition buckling was observed, confirming findings by Abramowicz and Jones [3].

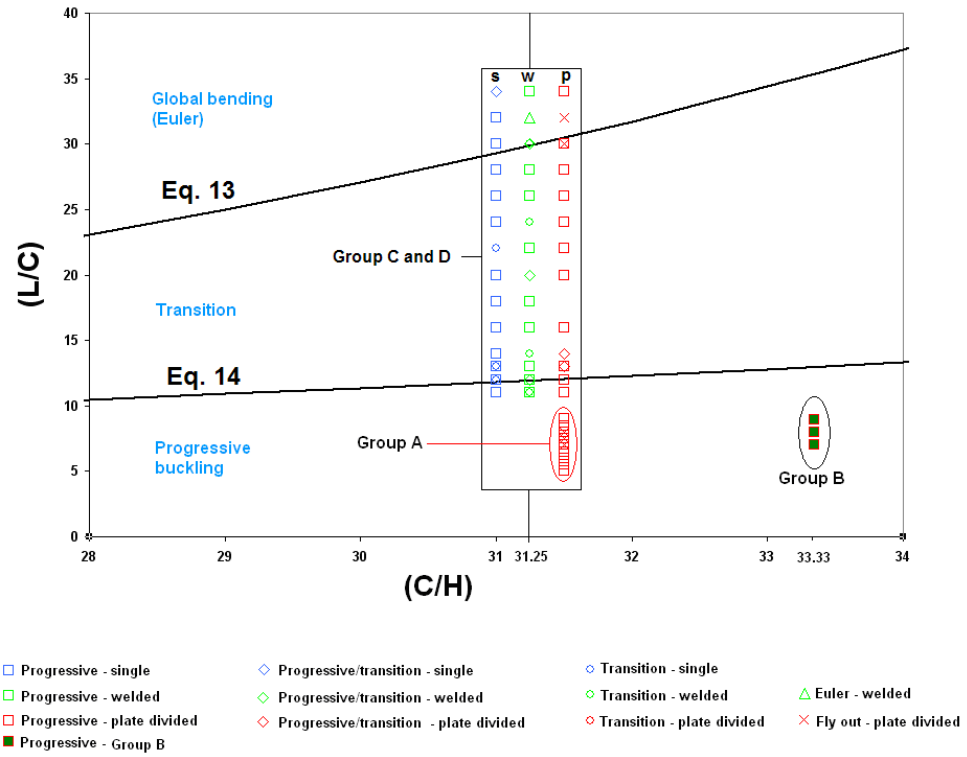

Figure 15 Length-to-width ratio versus width-to-thickness ratio graph showing dynamic test data compared to lines separating global plastic bending (Euler buckling) and local buckling (progressive buckling) obtained by Abramowicz and Jones [3].

4.2 Dynamic behaviour

As with quasi-static specimens, specimens in groups A, C and D had width-to-thickness ratios of 31.25 while those of Group B had width-to-thickness ratios of 33.33. For the width-to-thickness ratio 31.25 Abramowicz and Jones [3] predicted that transition buckling would occur in single tubes at about 600mm while global bending would occur at about 1500mm. As predicted by Abramowicz and Jones [3] in single tube specimens, transition buckling was first observed in a 600mm specimen. In welded specimens, transition buckling was first observed in a 550mm specimen. Global bending only occurred in one welded specimen, 800w800 (1600mm). Global bending was not observed in single tube specimens. In plate-divided specimens, transition and global bending did not occur as all the specimens buckled in a progressive manner. In 1500mm (750p750) and 1600mm (800p800) plate-divided specimens, fly-outs occurred after progressive buckling occurred. In general the axial displacements did not vary much between the three configurations and there was no consistency in terms of which configuration crushed more for a specific length, but holistically, plate divided specimens could be considered the better energy absorbers as they did not exhibit transition and global bending. Of the three tube configurations, welded specimens performed the worst as irregular folding and transition buckling occurred more often in these specimens. Any slight inaccuracy in lining up the tubes



Figure 16 Buckling profiles of 1100mm specimens with close-up of 1100s showing initial progressive buckling and subsequent global buckling characterising transition buckling.

when welded would cause buckling in the weld region or transition buckling to occur as a result of the geometric instability.

5 CONCLUDING REMARKS

The results from an experimental investigation into crushing characteristics of single, welded and plate divided mild steel tubes of varying lengths subjected to quasi-static and dynamic axial loading have been presented. In quasi-static tests force-displacement curves revealed that welded tubes behaved very similarly to single tubes in that they exhibited one peak load. The weld heat affected zone does not appear to act as a trigger for the buckling process. In plate-divided specimens, however, two ultimate peak loads were observed and in turn this slightly increased the mean load (about 1kN) experienced by the specimens compared to single and welded tube specimens.

In dynamic tests welded specimens display very similar crushing behaviour to single tubes but the weld may create a geometric instability in some cases which will lead to undesirable buckling modes. Lobe layers at the weld region would be slightly larger than lobe layers elsewhere along a specimen since the effective thickness at this point was slightly larger. In plate-divided specimens the frictional forces at the tubes and plate contact interfaces are not enough to overcome slight lateral movement of the plate and upper tube. This lateral degree of freedom in plate-divided specimens hinders the onset of transition or global bending and allows progressive buckling to take place.

From a manufacturing point of view, welded tubes and single tubes are comparable in

terms of energy absorption performance provided the total length to thickness ratio is within the progressive buckling regimes. While the plate-divided tubes are not suitable for horizontal deforming energy absorption system they may be useful for vertical applications such as base of lift shafts.

Acknowledgements The authors acknowledge the contributions of Mr G. Newins of the Department of Mechanical Engineering, University of Cape Town, for the preparation of the test specimens. Participation in this project would not have been possible without the financial support from the National Research Foundation of South Africa (NRF), and Armaments Corporation of South Africa (ARMSCOR).

References

[1] L. Abah, A. Limam, and M. Dejeammes. Effects of cutouts on static and dynamic behaviour of square aluminium extrusions. In *5th International Conference on Structures Under Shock and Impact, (SUSI V)*, pages 133–142, Southampton, UK, 1998. Computational Mechanics Publications.

[2] W. Abramowicz and N. Jones. Dynamic progressive buckling of circular and square tubes. *Int J Impact Eng*, 4(4):243–270, 1986.

[3] W. Abramowicz and N. Jones. Transition from global bending to progressive buckling of tubes loaded statically and dynamically. *Int J Impact Eng*, 19(5):415–437, 1997.

[4] A.A.A. Alghamdi. Collapsible impact energy absorbers: an overview. *Thin-Walled Structures*, 39(2):189–213, 2001.

[5] K.R.F. Andrews, G.L. England, and E. Ghani. Classification of the axial collapse of cylindrical tubes under quasi-static loading. *Int J Mech Sci*, 25(9/10):687–696, 1983.

[6] B. Arnold and W. Altenhof. Experimental observations on the crush characteristics of AA6061 T4 and T6 structural square tubes with and without circular discontinuities. *Int J Crash*, 9(1):73–87, 2004.

[7] S.B. Bodlani, S. Chung Kim Yuen, and G.N. Nurick. The energy absorption characteristics of square mild steel tubes with multiple induced circular hole discontinuities. Part I: Experiments. *J Appl Mech*, 76(4):041012–1–041012–11, 2009.

[8] Q. Cheng, W. Altenhof, and L. Li. Experimental investigations on the crush behaviouf of AA6061-T6 aluminium square tubes with different types of through-hole discontinuities. *Thin-Walled Structures*, 44(4):441–454, 2006.

[9] S. Chung Kim Yuen and G.N. Nurick. Modelling of axial loading of square tubes with blast-induced imperfections. In *Proceedings of 9th International Symposium on Plasticity and Impact Mechanics, IMPLAST 2007*, pages 553–560, Bochum, Germany, 2007.

[10] S. Chung Kim Yuen and G.N. Nurick. The energy absorbing characteristics of tubular structures with geometric and material modifications: an overview. *Applied Mechanics Reviews*, 61(2), 2008. 020802-1-020802-15.

[11] S. Chung Kim Yuen and G.N. Nurick. The response of large square tubes (width/thickness ratio > 45) to opposite lateral blast loads followed by dynamic axial load. In *IUTAM Symposium on Theoretical Computational and Modelling Aspects of Inelastic Media*, pages 309–317. Springer, 2008. ISBN 97814020 90899.

[12] S. Chung Kim Yuen and G.N. Nurick. The crushing characteristics of square tubes with blast-induced imperfections – Part I : Experiments. *J Appl Mech*, 76(5):051308–1–051308–16, 2009.

[13] S. Chung Kim Yuen, G.N. Nurick, and R.A. Starke. The energy absorption characteristics of double-cell tubular profiles. *Latin American Journal of Solids and Structures*, 5(4):289–317, 2008. ISSN 1679-7817.

[14] B.P. DiPaolo, P.J.M. Monteiro, and R. Gronsky. Quasi-static axial crush response of a thin-wall, stainless steel box component. *Int J Solids and Struc*, 41(14):3707–3733, 2004.

[15] N.K. Gupta and S.K. Gupta. Effect of annealing size and cutouts on axial collapse behaviour of circular tubes. *Int J Mech Sci*, 35(7):597–613, 1993.

[16] A.G. Hanssen, M. Langseth, and O.S. Hopperstad. Static and dynamic crushing of square aluminium extrusions with aluminium foam filler. *Int J Impact Eng*, 24(4):347–383, 2000.

[17] Ø. Jensen, M. Langseth, and O.S. Hopperstad. Experimental investigations on the behaviour of short to long square aluminium tubes subjected to axial loading. *Int J Impact Eng*, 30(9):973–1003, 2004.

[18] N. Jones. *Structural Impact*. Cambridge University Press, 1989.

[19] N. Jones. Several phenomena in structural impact and structural crashworthiness. *European Journal of Mechanics A/Solids*, 22(5):693–707, 2003.

[20] D. Karagiozova. Dynamic buckling of elastic-plastic square tubes under axial impact – I: stress wave propagation phenomenon. *Int J Impact Eng*, 30(2):143–166, 2004.

[21] D. Karagiozova and M. Alves. Transition from progressive buckling to global bending of circular shells under axial impact – Part I: Experimental and numerical observations. *Int J Solids and Struc*, 41(5/6):1565–1580, 2004.

[22] D. Karagiozova and M. Alves. Transition from progressive buckling to global bending of circular shells under axial impact – Part II: Theoretical analysis. *Int J Solids and Struc*, 41(5/6):1581–1604, 2004.

[23] D. Karagiozova and N. Jones. Dynamic buckling of elastic-plastic square tubes under axial impact – II: structural response. *Int J Impact Eng*, 30(2):167–192, 2004.

[24] D. Karagiozova and N. Jones. On the mechanics of the global bending collapse of circular tubes under dynamic axial load. dynamic buckling transition. *Int J Impact Eng*, 35(5):397–424, 2008.

[25] D.K. Kim, S. Lee, and M. Rhee. Dynamic crashing and impact energy absorption of extruded aluminium square tubes. *Materials and Design*, 19(4):179–185, 1998.

[26] M. Langseth, T. Berstad, O.S. Hopperstad, and A.H. Clausen. Energy absorption in axially loaded square thin-walled aluminium extrusions. *Structures Under Shock Impact III (SUSI III), CMP, Southampton*, pages 401–410, 1994.

[27] M. Langseth, O.S. Hopperstad, and A.G. Hanssen. Crash behaviour of thin-walled aluminium members. *Thin-Walled Structures*, 32(1/3):127–150, 1998.

[28] S. Lee, C. Hahn, M. Rhee, and J.E. Oh. Effect of triggering on the energy absorption capacity of axially compressed aluminium tubes. *Materials and Design*, 20(1):31–40, 1999.

[29] A.G. Mamalis, D.E. Manolakos, G.L. Viegelahn, N.M. Vaxevanidis, and W. Johnson. The inextensional collapse of grooved thin-walled cylinders of PVC under axial loading. *Int J Impact Eng*, 4(1):41–56, 1986.

[30] S.T. Marais, R.B. Tait, T.J. Cloete, and G.N. Nurick. Material testing at high strain rate using the split Hopkinson pressure bar. *Latin American Journal of Solids and Structures*, 1(3):319–338, 2004.

[31] N. Marshall and G.N. Nurick. The effect of induced imperfections on the formation of the first lobe of symmetric progressive buckling of thin-walled square tubes. In *Structures Under Shock Impact V (SUSI V)*, pages 155–168, Southampton, 1998. Computational Mechanics Publications.

[32] T.Y. Reddy and S.T.S. Al-Hassani. Axial crushing of wood-filled square metal tubes. *Int J Mech Sci*, 35(3/4):231–246, 1993.

[33] M. Seitzberger, F.G. Rammerstorfer, R. Gradinger, H.P. Degischer, M. Blaimschein, and C. Walch. Experimental studies on the quasi-static axial crushing of steel columns filled with aluminium foam. *Int J Solids and Struc*, 37(30):4125–4147, 2000.

[34] K.C. Shin, J.J. Lee, K.H. Kim, M.C. Song, and J.S. Huh. Axial crush and bending collapse of an aluminum/gfrp hybrid square tube and its energy absorption capability. *Compos Struc*, 57(1/4):279–287, 2002.

[35] V. Tarigopula, M. Langseth, O.S. Hopperstad, and A.H. Clausen. Axial crushing of thin-walled high-strength steel sections. *Int J Impact Eng*, 32(5):847–882, 2006.

[36] M.D. Theobald and G.N. Nurick. Numerical investigation of the response of sandwich-type panels using thin-walled tubes subject to blast loads. *Int J Impact Eng*, 34(1):134–156, 2007.